AvB

DebrisInterMixing-2.3: a finite volume solver for three-dimensional debris-flow simulations with two calibration parameters - Part 2: Model validation

Albrecht v. Boetticher[1,3], Jens M. Turowski[2], Brian W. McArdell[3], Dieter Rickenmann[3], Marcel Hürlimann[4], Christian Scheidl[5], and James W. Kirchner[1,3]

[1]Department of Environmental Systems Science, Swiss Federal Institute of Technology Zurich ETHZ, CHN H41, 8092 Zürich, Switzerland
[2]Helmholtz-Centre Potsdam GFZ German Research Center for Geosciences, Telegrafenberg, 14473 Potsdam, Germany
[3]Swiss Federal Research Institute WSL, Zürcherstrasse 111, 8903 Birmensdorf, Switzerland
[4]Department of Geotechnical Engineering and Geosciences, Technical University of Catalonia UPC, Jordi Girona, 1-3 (D2), 08034 Barcelona, Spain
[5]Institute of Mountain Risk Engineering, BOKU, Peter-Jordan-Straße 82, 1190 Vienna, Austria

Correspondence to: Albrecht v. Boetticher (albrecht.vonboetticher@usys.ethz.ch)

Abstract. Here we present validation tests of the fluid dynamic solver presented in v. Boetticher et al. (2016), simulating both laboratory-scale and large-scale debris-flow experiments. The new solver combines a Coulomb viscoplastic rheological model with a Herschel-Bulkley model based on material properties and rheological characteristics of the analysed debris flow. For the selected experiments in this study, all necessary material properties were known – the content of sand, clay (including its mineral composition) and gravel (including its friction angle) as well as the water content. We show that given these measured properties, two model parameters are sufficient for calibration, and a range of experiments with different material compositions can be reproduced by the model without recalibration. One calibration parameter, the Herschel-Bulkley exponent, was kept constant for all simulations. The model validation focuses on different case studies illustrating the sensitivity of debris flows to water and clay content, channel curvature, channel roughness and the angle of repose. We characterize the accuracy of the model using experimental observations of flow head positions, front velocities, run-out patterns and basal pressures.

1 Introduction

Debris flows are a frequent natural hazard in mountain regions. They consist of a mixture of water, clay, sand and coarser material traveling as a partly fluidized mass through steep channels. The mix of different materials leads to a complex rheological behavior that is still not well understood. Field observations of debris-flow behavior and rheology are challenging and still rare, and numerical modeling is often the approach of choice when assessment of debris-flow behavior is needed for planning, zoning, and hazard assessment (Scheuner et al., 2011; Christen et al., 2012). Most models require direct calibration to capture site-specific behavior. However, reliable calibration data are rare, and laboratory experiments cannot be perfectly scaled to field situations. v. Boetticher et al. (2016) recently presented a new solver that was designed for the simulation of debris flow be-

havior based on only two free model parameters. The model treats the air and fluid phase separately, and derives the properties of the latter by concentration-dependent mixing of a granular material fraction with a fine material suspension. The granular material fraction is modeled as a fluid with Coulomb-viscoplastic rheology and the fine material suspension is characterized by a Herschel-Bulkley rheology. The local rheology of the bulk mixture is obtained from the rheological properties of the

5 gravel and fine material suspension, as a linearly weighted average of the corresponding shares in the debris flow material. The composition is pre-defined, and no dynamic changes of the gravel concentration or of the share of fine material suspension are modeled at this stage. Material properties are related to the fractions of different minerals within the debris-flow material and to water content.

The object of this study is to illustrate the model's ability to accurately account for a wide range of flow behaviors without

10 recalibration. The key attributes of the model are its sensitivity to water content, gravel- and clay-fraction and clay-mineralogy on the one hand, and the interaction between the three-phase rheology and the complex three-dimensional flow structure on the other. We present some validation test cases and discuss limitations of the model set-up based on simulation results for intermediate and large-scale experiments.

2 Model validation and performance based on selected flume experiments

15 The model, as described by v. Boetticher et al. (2016), is based on an adaptation of the interMixingFoam solver of the open source finite volume code OpenFOAM (OpenFOAM-Foundation, 2014), in combination with a stable implementation of the pressure-dependent rheology model of Domnik et al. (2013) to describe the gravel phase as a Coulomb-viscoplastic fluid, combined with a Herschel-Bulkley rheology implementation for the interstitial slurry of water and fine sediment. In addition to determining typical material parameters (density, water content and relative amounts of gravel and clay), the user is required

20 to input the clay composition (e.g., the fractions of kaolinite and chlorite, illite, montmorillonite; (Yu et al., 2013)), and δ, the friction angle of the gravel fraction, as its angle of repose. The two remaining calibration parameters are related to the fine material suspension. One of the two free model parameters, the Herschel-Bulkley exponent n, was kept constant and set to 0.34, which was found to be a value suitable for all simulations presented here. The only parameter modified for calibration was τ_{00}, which acts as a restricted multiplication factor for the calculated yield stress of the fine sediment suspension.

25 Three different experimental setups were chosen to illustrate how sensitively the modeled flow and depositional processes react to changes in water- and clay content, channel curvature and bed roughness. The first experimental case used for validation is based on flume experiments from Hürlimann et al. (2015), simulating hillslope debris flows on a wide laboratory slope to exclude side-wall effects as suggested by Jop et al. (2008). We use this case study to illustrate that the calibrated model can predict flow behavior with different water contents without recalibration.

30 The second experimental case used for validation was designed to study the sensitivity of debris flows to channel curvature (Scheidl et al., 2015). The channel had a semi-circular cross-section and was composed of two curves with different radii. The experimental setup focused on surface super-elevation (lateral difference in flow surface elevation in a channel bend), and we consider it as suitable for verifying the modeled rheology of the mixture in channel bends.

While the two sets of experiments described above were performed with small amounts of sediment, over short times and at a laboratory scale, we also tested our model against data from full-scale experiments performed in the USGS experimental debris-flow flume at the H. J. Andrews Experimental Forest, Oregon (Iverson et al., 2010). In these experiments, debris flow material was released into a 2 m wide and about 75 m long flume with 31° inclination, followed by a smooth transition into a planar run-out area with a 2.5° slope in the flow direction. In the initial experiments, the channel was a flat concrete bed; in later experiments, the bed was paved with 1.6 cm high bumps.

The model setup and performance for all three cases are described in more detail in the following sections.

2.1 Boundary conditions and release setup

The mobilization of debris flow material in nature is linked to a change in water content and pore pressure and a corresponding state-dependent transient weakening (Iverson et al., 1997). The focus of this work is not on the release process but on the capability to predict runout distances and impact pressures, and instead of a natural mobilization, the selected experiments released material by opening a head gate. We performed our simulations without a gate as sudden dam-break releases and compared them to simulations including the dynamic motion of the gate. In the first case study the gate was removed vertically in a fast upward motion (Fig. 1), while at the USGS flume a gate consisting of two wings was unlocked and pushed open by the material. Although the gate opening had an effect on the formation of the front flow depth, the difference between simulations with or without the gate vanished during the flow process prior to reaching points of measurements that we used for comparison (Fig. 2 and 3). A no-slip boundary was applied in all simulations, which is only appropriate in situations with high contents of fine material where viscoplastic behavior dominates. The application of a no-slip boundary condition to the USGS flume experiment with a sand-gravel mixture (called SG mixture in the following) on a smooth bed does not fulfill this requirement and was only chosen to have a model setup which is comparable to the sand-gravel mixture with loam (called SGM mixture in the following). The SG mixture was modeled to see how the model performs at its limit of applicability.

2.2 Experimental validation of water content sensitivity

In our modeling approach, the rheology of the slurry phase (fine material suspension) depends on its yield stress, which is known to be exponentially dependent on water content (e.g., Hampton (1975), O'Brian and Julien (1988), Yu et al. (2013), Hürlimann et al. (2015)), with increasing exponents for higher clay fractions. Therefore, for each material composition there should be a critical range where a minor variation in water content causes a strong change in flow depths and run-out distance. Three experiments from Hürlimann et al. (2015) were selected, lying within the range of high water-content sensitivity. These debris-flow experiments were carried out by releasing $0.01\,\mathrm{m}^3$ of debris flow material from a 0.4 m wide reservoir into a 4.4 m long and 2 m wide, 30° inclined plane followed by a 2.5 m long, 2 m wide and 10° inclined run-out section (Fig. 1). The flume was covered by a rubber layer with a burling consisting of flat circular discs of 4 mm diameter and about 0.3 mm height every 5 mm to increase roughness. The experimental sediment mixtures used for model validation only differed in water content (27.0%, 28.5%, and 30.0% by weight) and contained about 1.6% smectite, 8.8% other clay minerals, 27.8% silt, 47.7% sand and 14% gravel. The corresponding wet bulk densities were 1822, 1802 and 1722 $\mathrm{kg/m}^3$.

All selected experiments were simulated using the same value of $\delta = 36°$ for the angle of repose of the gravel mixture. This friction angle was determined in a simple adaptation of the method of Deganutti et al. (2011) by tilting a large box with loose material until a second failure of the material body occurred. The model parameter τ_{00} was calibrated to fit the observed run-out length of the 28.5% water content experiment, and the two tests with 1.5% higher or lower water content were used to

5   validate the sensitivity of the model to water content.

The model adapts to a new water content by calculating a new Herschel-Bulkley yield stress (see v. Boetticher et al. (2016)). However, the free model parameter τ_{00} should be adapted to the new water content as well. Let τ_{y-cal}^{w-new} be the Herschel-Bulkley yield stress calculated by the model for a new water content, but based on the original value of the calibration parameter τ_{00-cal} that is not yet adjusted to the new water content. Due to the need to account for the influence of a different water content on

10   the free model parameter τ_{00}, some user action is necessary. The free model parameter τ_{00} is reduced or increased according to equation 1,

$$\tau_{00} = \tau_{00-cal} \frac{\tau_{y-cal}^{w-new}}{\tau_{y-cal}}, \tag{1}$$

to obtain a rheology with all parameters adapted to the new water content, where τ_{00-cal} and τ_{y-cal} denote the free model parameter value and the corresponding Herschel-Bulkley yield stress calculated by the model in the calibration test. This way,

15   the change of the yield stress initially calculated by the model is also applied to the free model parameter τ_{00}.

Based on the calibrated value of $\tau_{00} = 41.3$ Pa for an experiment with 28.5% water content (the calibration test), the rheologies of the two mixtures with 1.5% higher or lower water content were calculated using equation 1. For a water content of 27.0% (subsequently denoted as the reduced water experiment) this procedure resulted in $\tau_{00} = 51.8$ Pa, whereas for the 30% water content (denoted as the increased water experiment in the following) the result was $\tau_{00} = 21.3$ Pa. For each of

20   the three experiments, laser-measured flow depths were available in the center of the flume, one meter downslope of the gate. Comparisons between measured and simulated flow depths at such small scales are only approximate due to the surface disturbance by coarser grains that cause significant fluctuations in surface elevation. However, the arrival time, the maximal flow depths and the decay of surface elevation over time were considered to be suitable for comparison to the model. The model performance was evaluated by comparing the deposition patterns, travel times, and time series of flow depths in the

25   simulations and experiments. The simulated flow depths reproduce the laser signal with respect to both time and amplitude (Figure 4) and predicted run-out deposits replicate the water content sensitivity (Figure 5). Although the front arrival of the reduced water test is delayed by 0.2 s in the simulation, the maximum flow depth is reached at the same time in the experiment and simulation (Figure 4 top). The maximum flow depth is accurately predicted by the model, with a deviation of 2 mm, which is less than the average gravel grain size. The fast decrease of the measured surface elevation within 0.1 s after the peak is

30   well captured by the model, followed by a moderate decrease until 1.2 s. At this point, in the experiment with reduced water content a transition began towards the stable level of about 11 mm flow depth, which corresponds to the maximum grain size. This transition begins later in the simulation and declines further to a modeled final deposit of 6 mm thickness; however, large measured fluctuations of flow depth are likely due to the coarser grains present in the test. The predicted deposit length of

2.42 m in the simulation overestimates the experimental value of two meters (Figure 5 top). However, the simulated front also temporarily paused at x = 2.04 m, until it was overrun by a second wave 0.1 s later. There is an almost perfect fit between the shapes of the experimental and simulated deposits in the calibration case (Figure 5 center). The maximum flow depth and the subsequent decrease are well reproduced (Figure 4 center), although the front arrival time at the laser is again delayed by

5   some 15 %. The measured and simulated flow depth in the wet experiment show that the early front arrival time and the time of the maximum flow depth are precisely predicted by the model. The moderate decrease of the surface elevation over time is captured by the model (Figure 4 bottom), although the maximum flow height is underestimated. The final deposit thickness of about 4 mm at the laser is reproduced correctly but the run-out length of 5.17 m is over-predicted by about 7% compared to the experimental value of 4.84 m (Figure 5 bottom).

10 **2.3   Non-Newtonian rheology in channel bends: Evaluation of surface super-elevation due to curvature**

Enhanced super-elevation due to curvature is characteristic for viscous debris flows (Wang et al., 2005; Bertolo and Wieczorek, 2005), so it can be viewed as a further indicator for model quality. As we expect the enhanced super-elevation of debris flows in curved channels to be connected to a change of viscosity due to the pressure increase caused by deflection within the curve, the second group of experiments focuses on the pressure-dependent rheology. With β as the average surface inclination transverse

15 to the flow direction, a correction factor k^* can be defined as the ratio between the gradient $tan(\beta)$ of super-elevation of debris flow material and the corresponding gradient of clear water with the same average flow velocity. Based on the forced vortex approach with the assumption of a constant radius of the channel bend, Scheidl et al. (2015) investigated the effect of flow velocity and super-elevation for several debris flow mixtures.

    The experiments were performed by releasing 0.0067 m^3 of material from a reservoir, through a transitional "box-to-

20 channel" reach, into a channel of half-circular cross-section with 0.17 m diameter and a constant downslope channel inclination of 20° (Scheidl et al., 2015). The channel was arranged in an S shape, with a first 60° curve to the left with 1.5 m curve radius followed by a second curve to the right with 1 m curve radius (Fig. 6). The channel was covered with sandpaper to increase roughness.

    Here, we consider the mixture with the largest clay content (mixture A of Scheidl et al. (2015)) where less demixing and

25 phase separation was observed, and focus on the first curve of 1.5 m radius. The flow height in a cross section, two-thirds of the way through the curve, was measured by three lasers across the channel (Fig. 7). The arrival time at the laser section could not be used as a criterion for model calibration, because a simplification of the box-to-channel reach was necessary. This was due to the fact that the complex geometry at the transition to the channel (Fig. 6 region (d)) caused local air inclusions. A very fine grid resolution would be necessary here to adequately simulate the immediate demixing of the air. Therefore, as a

30 simplification in our model set-up, the straight channel section was extended to the reservoir where it was filled with material at rest. Thus, the measured travel times between the gate and the first lasers are not comparable to those in the model. Instead, the free model parameter τ_{00} was calibrated to correctly predict the front velocity at the laser section. This front velocity was determined from high-speed video recordings. The average value from all experiments with mixture A at the upper curve was 1.49 m/s, leading to $\tau_{00} = 26$ Pa to reach the same flow front velocity in the simulation. Mixture A was composed of 6.5%

clay, 15% silt, 26.1% sand and 52.4% gravel by dry weight. Since the gravel phase in the experiment was created from the same gravel as used in section 2.2, a value of $\delta = 36°$ was applied here, too. The water content was 27% and the density of the mixture was about $1800\,\mathrm{kg/m^3}$.

The measured and simulated surface deflections can be compared to assess how well the modeled rheology accounts for the increased super-elevation. Nevertheless one should be aware that in this experimental setup, a granular front developed, which is in contradiction to the homogeneous phase distribution in the current implementation (Fig. 7 right). The laser at the inside of the curve did not always register any material in the experiments or simulation, so the gradient of the super-elevation angle, $tan(\beta)$, is reconstructed from the simulation once as $tan(\beta_{max})$ by using the points of maximal surface elevations at the inside and outside of the flow (P_i and P_o in Fig. 7), and once as $tan(\beta_{min})$ based on the elevations of laser 2 and laser 3. At the moment of maximum surface elevation, the modeled $tan(\beta_{max})$ equals 0.336, resulting in $k^* = 2.11$ as defined by Scheidl et al. (2015), which fits the experimental average of 0.33 (Scheidl et al. (2015) table 2) and the correction factor $k^* = 2.1$. The corresponding value for $tan(\beta_{min})$ reaches 0.243, underestimating the experimental values; however, the corresponding correction factor k^* equals 1.52 and still lies within the experimental standard deviation. The surface super-elevation is captured by the model although the front volume is underestimated by more than 50%. The under-predicted volume is a consequence of both the simplified geometry of the release area and the continuous over-prediction of material losses at the channel margins where material becomes immobile due to the no-slip boundary condition, whereas in the experiment little material was deposited at the wall because the walls were moistened prior to the experiment. This problem needs to be addressed before more detailed comparisons can be made. Nevertheless this example is included to illustrate that the model can predict plausible degrees of superelevation.

2.4 Large scale experiments: Effects of bed roughness and share of fine material

Because it is difficult to upscale from laboratory-scale tests to true debris flow events, large-scale debris flow experiments are essential for model validation. The USGS debris-flow flume consists of a 75 m long, 2 m wide and 31° inclined concrete channel, with a release reservoir having the same width and slope, and an approximately 7.5 m long distal reach where the bed inclination forms a smooth transition to a run-out plane with a 2.5° inclination and no lateral confinement (Iverson et al., 2010). Laser sensors measure the flow height 32 m and 66 m downslope from the release gate, and a third laser is located in the run-out plane. The flume is tilted to one side, and the maximum tilt reaches 2°. The model accounts for this with a 1° tilt over the whole flume length.

We selected three experimental setups, two to illustrate the model capabilities and one that has a material composition where the model is only applicable with restrictions. The model cannot account for grain collisions and therefore is limited to debris flow mixtures which contain significant amounts of muddy suspension with a high loam content. The two first setups focus on experiments with released material consisting of the so-called SGM mixture Iverson et al. (2010), which is composed of 2.1% clay, 4.9% silt, with 37% sand and 56% gravel (by dry weight). Following James and Bait (2003), we assume that kaolinite dominates the clay minerals, although smectite could be present. We have chosen an SGM-mixture experiment with

a documented runout deposit, and with a smooth channel bed surface to reduce the influence of granular collisions. The other setup should illustrate the interplay with the pressure-sensitive representation of the gravel, so a rough channel bed was used.

An important element of our simulation is that we compare the model with the channel experiments based on the calibration with respect to the arrival time of the flow front. Additional simulations that illustrate the model performance for simulating the so-called SG-mixture Iverson et al. (2010) and the corresponding flow on smooth channel beds were conducted without recalibration, based on the calibration for the rough channel SGM-mixture experiments (Fig. 8). The SG-mixture has no clay and is composed of 1% silt, 33% sand and 66% gravel.

2.4.1 Smooth channel experiment with high content of loam

The selected experiment was documented by (Major, 1997) as a release of 9 m^3. The water content and density of this test were determined as 18.5% and 1761 kg/m^3, respectively, by assuming fully saturated material. The angle of repose was estimated to be 39.3° on the basis of tilt table tests of the SGM mixture (Iverson et al. (2010)). The experiments were documented by videos and by surveys of the runout deposits (Logan and Iverson, 2013). The model parameter $\tau_{00} = 90$ Pa was calibrated such that the time between release and front arrival at the run-out plane matched the experiment. Both the run-out process and the final deposit therefore contributed to the model validation, because they were not considered for the calibration. The simulated spreading into the run-out plane evolved in good agreement with the experimental observations (Fig. 9). In the experiment, several surges arrived at the run-out plane after the time sequence shown in Figure 9, widening the material deposit at the foot of the channel. By contrast, the model evolved in a single surge. The maximum deposit length on the run-out plane in the experiment was 15 m and the simulated front reached 14 m.

2.4.2 Rough channel experiment with high content of loam

The SGM mixture was applied in the rough channel experiments with 17.9% water content and 2010 kg/m^3 density (based on Iverson et al. (2010) table 2). The angle of repose was estimated to be 39.6° on the basis of tilt table tests of the SGM mixture (Iverson et al. (2010), see column (SGM) in table 3).

For the rough channel experiments, round-nosed cones as bumps of 1.6 cm height were installed on the bed every 5 cm; these were introduced in the model as pyramids as a trade-off between resolving the bed roughness and limitations of grid resolution due to numerical costs (Fig. 10). Flow depth and basal force measurements were available as averaged values over a set of experiments with identical releases and channel setups, where the SGM material mixture (Iverson et al. (2010)) forms a 9.7 m^3 release body of known geometry. Three SGM experiments published by Iverson et al. (2010) with different flow front velocities were selected for front position comparison. A test from the year 2000, test 000928, represented an extreme case with a quite low front velocity in the beginning followed by a sudden speedup of the flow front after 6 seconds. The other two tests also showed a sudden acceleration of the flow front, but their release process was faster and the sudden change in front velocity appeared later and was less dominant (Fig. 12). To some extent the difference in front position over travel time seems to be due to a large second surge that originates from the reservoir (Fig. 13). Especially in test 000928, part of the material left

the reservoir with a delay, but as the second surge arrived at the front, the material front velocity doubled from about 8 m/s to 16 m/s.

The rough channel experiments with the SGM mixture were modeled with $\tau_{00} = 82.8$ Pa, leading to good agreement of the modeled flow front with the flow depth measurements at 32 m (see Fig. 15 a). In addition to the average friction angle derived from tilt table tests, a second simulation with a friction angle corresponding to the lower limit of measured friction angles was carried out. In this way, while keeping the value of the lower friction angle within the range of realistic values, we intend to balance out the overestimated roughness of the bumps by their modeled representation as pyramids. Both simulation results, i.e. $\delta = 39.6°$ and $\delta = 36.6°$, are shown in the diagrams to demonstrate that the effect is relatively small.

Flow front position, shape and surface wave patterns (derived from video recording) were compared to the corresponding simulations (Fig. 12 and Fig. 14), indicating a good agreement in front position and a comparable pattern of the small surface waves. The simulation with reduced gravel friction angle showed better agreement in the decelerating part of the flume, as expected. In the upper part of the flume, the modeled front seems to proceed too fast, which is due to the neglected gate opening process. However, a comparison of the modeled flow depths with the ensemble-averaged laser signal from all eight published SGM experiments 32 m downslope from the release gate shows that the simulated front arrived without any time delay (Fig. 15 a). Further downstream, at 66 m downslope, there is a discrepancy in measured and simulated front arrival times (Fig. 15 b), but the corresponding measured and simulated basal pressures fit well, especially for the simulation with a reduced gravel friction angle (Fig. 15 d). The flow depths generally developed within the standard deviation range of the measured values at 32 m, except at the late tail of the flow after 8 s from release, where both simulations resulted in some overestimation corresponding to two slow surface waves passing. The simulation with the smaller friction angle of $\delta = 36.6°$ reduced the oscillation of flow depths compared to the simulation with the larger gravel friction angle. The measurements of three force plates installed at 31.7, 32.3 and 32.9 m were averaged over all eight SGM experiments and compared with the pressure in the corresponding cells of the simulation (Fig. 15 c), and the same was done for the basal force measurements at position 65.6 66.2 and 66.8 m (Fig.15 d). The model initially overestimates the pressure fluctuation, probably due to the simplified representation of the bumps at the bed as pyramids. However, after 7 s of flow the modeled basal pressures lie within the standard deviation of the measured values.

3 Discussion

This study represents an attempt to develop a widely applicable modeling framework for debris-flow simulations, based on rather simple constitutive equations describing the two-phase flow rheology and combined with traditional 3D CFD modeling. Nevertheless the results are surprising, as it appears to be possible to produce accurate front velocities, flow depths and run-out distances for the different material compositions and experimental setups by calibrating only one of the two free model parameters.

3.1 Modeled water content sensitivity

The simulations of the small-scale experiments that focus on water content sensitivity could reproduce the pronounced dependency of the run-out length on water content. The model could predict flow depth developments over time. Some short-time peak deviations between observations and simulations reached values close to the maximum grain size, possibly resulting from

5   single grain effects. A slight overestimation of the influence of the higher water content led to a run-out over-prediction by 7% in the model compared to the observation. The deposit of the calibration test case was accurately reproduced by the model, but the run-out of the reduced water content experiment was over-predicted by 21%. This discrepancy might be reduced with better grid resolutions, because the simulated front for the reduced water content experiment came to a halt at the correct position but was overrun by a second pulse of material, leading to an unrealistic air inclusion within the simulated front. The absence

10   of discrete particles in the model allows the second pulse to pass over the front without any roughness elements. The same limitation by grid resolution and by the absence of particles becomes apparent when looking at the simulated run-out tip of the experiment with increased water content. Due to the large stretching of the material, the flow front depth was represented by less than five grid cells, resulting in an inaccurate velocity profile and shear gradient, and thus leading to an imprecise viscosity. Furthermore, the interface thickness of the Volume Of Fluid approach at such low grid resolutions in relation to flow

15   depth leads to significant air phase concentrations over the whole flow depth of the front. This results in a reduced density and viscosity at the flow front.

3.2 Enhanced super-elevation in channel bends

The results of the curved channel experiments are encouraging, but further research is needed to evaluate whether the super-elevation of the surface due to channel curvature can be represented with such accuracy for other mixtures and at the lower

20   channel bend. The focus on a mixture of high clay content was due to the fact that our simplified solver cannot account for phase separations due to grain-size sorting. The upper curve was chosen to save computational time. However, the non-Newtonian behavior resulting in increased super-elevation was more pronounced for mixtures with less clay content and slower front velocities at the lower curve. From the results obtained at the upper curve, we may at least conclude that the model can reproduce enhanced super-elevations and seems to be suitable to predict debris-flow breakouts in curved channels for hazard

25   assessment. The main limitation is that the maximum cross-sectional area of the simulated flow reaches only about 40% of the area determined from the experiments. We severely underestimate the debris flow volume at the curve due to the simplified release geometry and due to material sticking to the walls in the model by the no-slip boundary condition, which in reality stayed mobile due to a wetting of the walls before the release. Therefore, an improved mesh including the reservoir and the box-to-channel reach is necessary before addressing the flow in the lower curve, which is beyond the scope of this paper.

3.3 Simulation of large scale experiments with high and low content of fine material on a smooth and a rough channel bed

The large-scale experiments at the USGS flume were chosen as examples of flows closest to prototype conditions of the real world, with relatively small uncertainties concerning material composition, flow front velocity or run-out patterns. The

5 experimental flow behavior was well captured by the model. In particular, the model successfully adapted from a mixture of 2.1% clay, 4.9% silt, with 37% sand and 56% gravel without recalibration to a material mixture without clay containing 1% silt, 33% sand and 66% gravel, combined with a severe change of channel roughness.

For the smooth channel bed, the spreading into the run-out plane was examined in detail. In both the experiment and the simulation, the front arrived at the experimental maximum deposit length in comparable time, for both the so-called SG

10 mixture and the SGM mixture (see Fig. 9 and 8). Although this indicates the model captures the deceleration process with some precision, the lack of grain size sorting in the model clearly becomes apparent and viscous tail surges are not covered. However, the modeled material deposition thickness in the SGM experiment with a smooth channel bed is comparable with the experimental deposit in the front regions that were only covered by the first two surges (Fig. 9).

Three experiments of identical setup using the SGM mixture together with a rough channel bed were selected to compare

15 flow front velocities with the simulation. Ensemble-averaged time evolutions of flow depths and basal pressures of eight such experiments were compared to the model output. The simulated flow depths lie in general within the range of standard deviations of the measurements. However, considering the basal pressures, part of the deviations between experiment and simulation may arise from the pyramid representation of the bumps (round-nosed cones) in the rough channel bed, leading in the model results to overestimated pressure peaks and thereby to an exaggerated viscosity by the pressure-dependent gravel

20 rheology. A reduced friction angle therefore improved the modeled flow front velocity, although the effect is not visible in the basal pressure fluctuation. The measured and simulated values do not agree with the mean arrival times implied by the laser signal at position 66 m (Fig. 15 b), however, they do by means of basal pressures for the lower gravel friction angle simulation (Fig. 15 d). As stated in Iverson et al. (2010), the laser data were less suitable for arrival time estimates compared to the force plates, because the granular flow front included single grains that bounced ahead and were captured by the laser before the

25 arrival of the dense material mixture. Because grain-size sorting effects and the release in two surges are not accounted for, a single surge flow forms in the simulation, in contrast to the real tests where two surges formed in most of the experiments considered. Therefore, when the modeled debris flow reaches the end of the channel, the front composition and volume is not an adequate representation of the experiment. As a consequence we did not model the run-out patterns of the rough channel experiments, in contrast to the smooth channel experiment where less demixing occurred.

30 On the one hand, it might be possible to obtain better representations of all SGM experiments with the current model by varying τ_{00} or density, water content, or the friction angle within the range of the published standard deviations of the experimental setup. On the other hand, we preferred to illustrate the model reliability based on input derived from averaged measurements to avoid unrealistic expectations that cannot be fulfilled in practice. To alter the level of detail, it would be more appropriate to include grain-size sorting effects.

3.4 Advantages and limitations of the model

Our approach allows the model parameters to be linked to material properties and local topography. It suggests that one should be able to develop a model that can be applied to a wide range of debris-flow simulations, wherever the necessary data on material and site conditions are available. The purpose was not to gain a perfect representation of the experiment, but to see how the chosen rheology represents the sensitivity to water content, channel roughness and curvature, and fraction of fine material. The new model overcomes a weak point of debris flow modeling: debris flow models commonly depend on many free parameters or are simplified by either modeling the flow from a granular perspective neglecting the interstitial fluid, or as a viscous continuum without accounting for the granular component of the flow process. Two-phase approaches, on the other hand, involve high numerical costs. In the case of two-phase coupling by drag between grain and fluid, the uncertainty in the drag between granular and fluid phases necessitates parameters that are difficult to quantify in case of the non-Newtonian suspension and non-spherical gravel grains. As a consequence, no previous modeling approach has succeeded in predicting debris-flow behavior across such different experimental settings as those examined here, with modifications to only a single parameter. Beyond that, our model succeeded in simulating different material mixtures without recalibration. However, numerical costs are still high for accurate results. The application is suitable for situations where the detailed flow structure is required. While the simulation of the smooth channel debris flow experiment at the USGS flume required seven hours per second of flow using 32 processors on the WSL Linux cluster HERA (consisting of Six Core AMD Opteron 2439 at 2.8 GHz), the rough channel experiment demanded ten hours per second of simulated flow and 44 processors due to the high grid resolution. However, these estimates are conservative because we did not have exclusive use of the computing power of the cluster during these tests.

4 Conclusions

The three-dimensional solver DebrisInterMixing-2.3 (v. Boetticher et al., 2016) combines a Coulomb viscoplastic rheological model for the solid phase with a Herschel-Bulkley model for the fluid phase for debris flow modeling. Here we describe validation tests of the solver. Based on published experiments we show that it is possible to calibrate the model using measurable properties of the material and two parameters, the Herschel-Bulkley exponent and the yield stress τ_{00}, which may require calibration. The Herschel-Bulkley exponent was held constant for all simulations.

We demonstrated the wide range of applicability of our new numerical debris-flow model. The model concept follows the strategy of shifting from requiring user expertise in debris flow model calibration towards requiring information about the modeled site. The presented simulations of a wide range of different experiments lead to the following conclusions:

1. The material mixture can be characterized based on clay mineral composition, proportions of clay, silt, sand and gravel, angle of repose of the gravel, and water content. For debris flows with a high content of fine material, a single free parameter allows calibration to adjust the model to the grid resolution.

2. The model can account for changes in the material mixture and water content without recalibration.

3. The model can account for the sensitivity of the rheology to channel geometry, including the enhanced surface super-elevation of debris flows in curved channels.

4. The sensitivity to surface roughness is captured by the model and it can be varied without recalibration.

The need to calibrate only one parameter in this study greatly simplified the model calibration process. For flows with large
5   proportions of fine material, the Herschel-Bulkley exponent may be chosen constant as well, which can save significant time
in the calibration process while still providing a highly detailed and reliable model. Although such a minimally parameterized
model may fit the real-world data less well than a highly parameterized model (perhaps because the latter is over-fitted), the time
saved in calibration can be used to explore a wider range of material composition and site properties. Because such changes in
model setup are translated into consequences for the flow physics by the model, the ensemble of such simulations may mirror
10   how the modeled site would respond to similar changes. Recalibrated models cannot deliver such information. Furthermore,
in our model there is less room for the user to make arbitrary parameter settings than in models with several calibration
parameters. Thus it may be possible to quantify the model's reliability in a robust and general way, because different users
are likely to apply comparable parameter settings. However, one missing element is phase separation due to grain-size sorting
effects, which would not only enable simulation of the granular front but also could enhance the model's capability to perform
15   channel bed erosion by mobilizing gravel deposits. This extension may be included in future versions of the model.

5   Code availability

The source code can be downloaded from the supplement application.zip; please follow the instructions given in the README.pdf
file for installation.

References

Bertolo, P. and Wieczorek, G. F.: Calibration of numerical models for small debris flows in Yosemite Valley, California, USA, Natural Hazards and Earth System Sciences, 5, 993–1001, 2005.

Christen, M., Bühler, M., Bartelt, P., Leine, R., Glover, J., Schweizer, A., Graf, C., McArdell, B. W., Gerber, W., Deubelbeiss, Y., Feistl, T., and Volkwein, A.: Integral hazard management using a unified software environment: numerical simulation tool "RAMMS" for gravitational natural hazards, in: 12th Congress INTERPRAEVENT, Proceedings Vol. 1, pp. 77–86, International Research Society INTERPRAEVENT, Grenoble, France, 2012.

Deganutti, A., Tecca, P., and Genevois, R.: Characterization of friction angles for stability and deposition of granular material, in: Italian Journal of Engineering and Environment: 5th International Conference on Debris-Flow Hazards: Mitigation, Mechanics, Prediction and Assessment, pp. 313–318, Padua, Italy, 2011.

Domnik, B., Pudasaini, S., Katzenbach, R., and Miller, S.: Coupling of full two-dimensional and depth-averaged models for granular flows, J. Non-Newton. Fluid Mech, 201, 56–68, 2013.

Hampton, M.: Competence of fine-grained debris flows, Journal of sedimentary petrology, 45, 834–844, 1975.

Hürlimann, M., McArdell, W., and Rickli, C.: Field and laboratory analysis of the runout characteristics of hillslope debris flows in Switzerland, Geomorphology, 232, 20–32, doi:10.1016/j.geomorph.2014.11.030, 2015.

Iverson, R. M., Reid, M. E., and LaHusen, R. G.: Debris-flow mobilization from landslides, Annu. Rev. Earth Planet. Sci., 25, 85–138, 1997.

Iverson, R. M., Logan, M., Lahusen, R. G., and Berti, M.: The Perfect Debris Flow? Aggregated Results from 28 Large-scale Experiments, J. Geophys. Res., 115(F03005), 2010.

James, M. and Bait, K.: Geologic Interpretation of Floodplain Deposits of the Southwestern Willamette Valley, T17SR4W With Some Implications for Restoration Management Practices Eugene, Oregon, James Geoenvironmental Services and Eugene District BLM, 2003.

Jop, P., Forterre, Y., and Pouliquen, O.: Crucial role of side walls for granular surface flows: consequences for the rheology, J. Fluid Mech., 541, 167–192, 2008.

Logan, M. and Iverson, R.: Video Documentation of Experiments at the USGS Debris-Flow Flume 1992–2006, Website U.S.Geological Survey Open-File Report 2007-1315, v. 1.3, http://pubs.usgs.gov/of/2007/1315/, visited 05.02.2014., 2013.

Major, J.: Depositional processes in large-scale debris-flow experiments, Journal of Geology, 105, 345–366, 1997.

O'Brian, J. and Julien, P. Y.: Laboratory analysis of mudflow properties, J Hydraul Eng, 114, 877–887, 1988.

OpenFOAM-Foundation: OpenFOAM Standard Solvers, Website User Guide of OpenFOAM, http://www.openfoam.org/docs/user/standard-solvers.php, visited 08.09.2014., 2014.

Scheidl, C., McArdell, B. W., and Rickenmann, D.: Debris-flow velocities and superelevation in a curved laboratory channel, Can. Geotech. J., 52, in print, 2015.

Scheuner, T., Schwab, S., and McArdell, B. W.: Application of a two-dimensional numerical model in risk and hazard assessment in Switzerland, in: 5th international conference on debris-flow hazards mitigation: Mechanics, Prediction and Assessment, pp. 993–1001, Padua, Italy, doi:10.4408/IJEGE.2011-03.B-108, 2011.

v. Boetticher, A., Turowski, J. M., McArdell, W. B., Rickenmann, D., and Kirchner, J. W.: DebrisInterMixing-2.3: a finite volume solver for three-dimensional debris-flow simulations with two calibration parameters – Part one: Model description, Geoscientific Model Development, 9, 2909–2923, doi:10.5194/gmd-9-2909-2016, 2016.

Wang, Z. Y., Wang, G. Q., and Liui, C.: Viscous and Two-Phase Debris Flows in Southern China's Yunnan Plateau, Water International, 30, 14–23, 2005.

Yu, B., Ma, Y., and Qi, X.: Experimental Study on the Influence of Clay Minerals on the Yield Stress of Debris Flows, J. Hydraul. Eng., 139, 364–373, 2013.
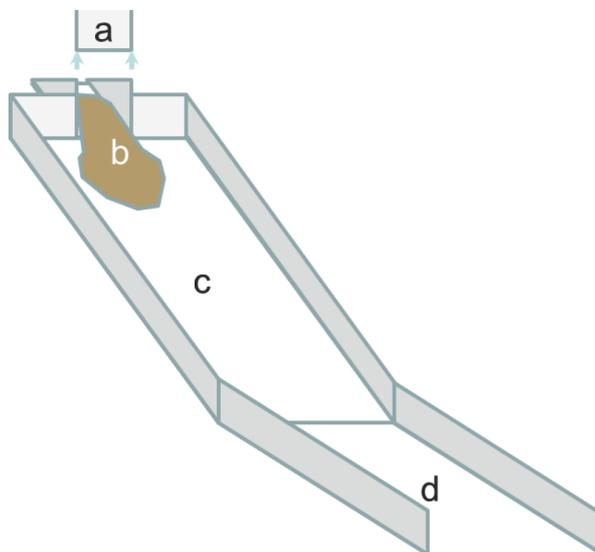
Figure 1. Isometric sketch of the hill slope debris-flow flume. Material (b) is released from the reservoir at the top by a sudden vertical removal of a gate (a) and flows down a steep slope (c) followed by a gently inclined run-out plane (d).
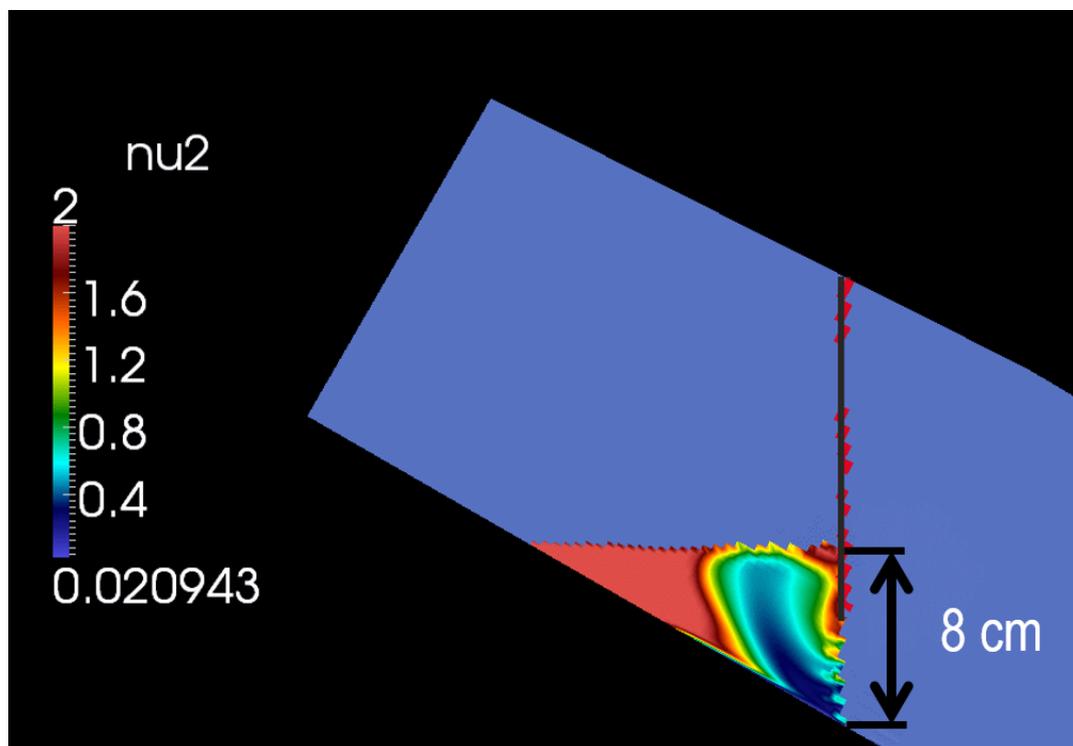
Figure 2. Longitudinal section through the hillslope debris-flow simulation 0.1 s after release including a vertical gate. The material is colored by the viscosity of the fine suspension illustrating the effect of the gate (vertical black line) which at that time was about 5 cm open and moved upward with 1 m/s (corresponding cell velocity colored in red). A body-force approach was used to account for the gate, which imposes forces on the fluid at cells that are in contact with the gate. These body forces are calculated in each time step based on Newton's second law to accelerate the fluid until it reaches a velocity equal to the body in motion.
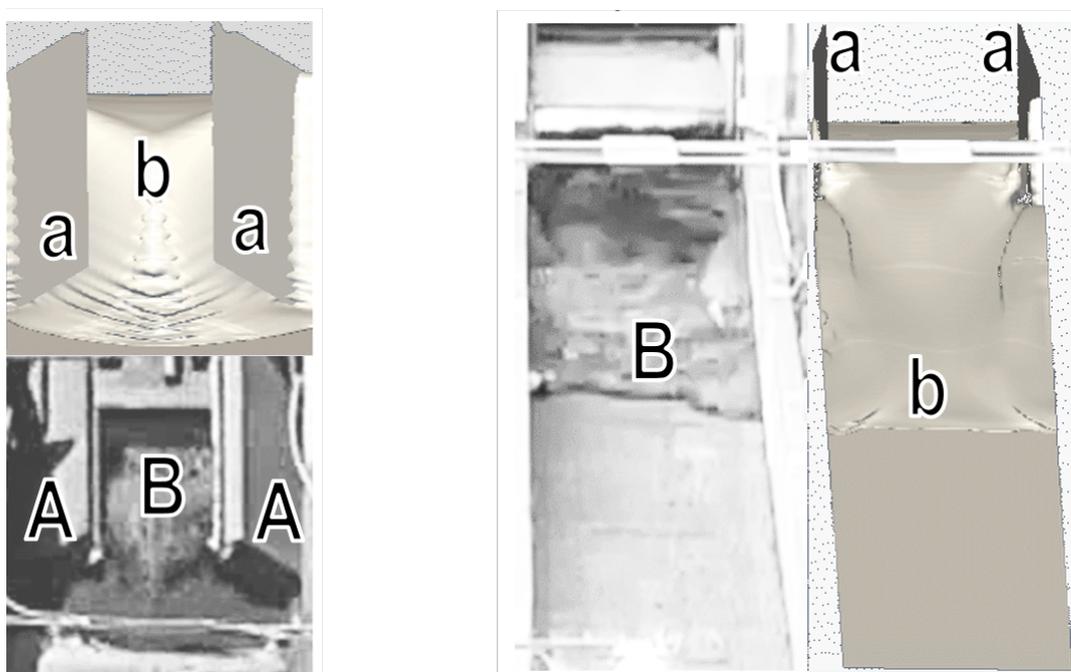
Figure 3. Screenshots comparing the modeled release, including the gate at the USGS flume, to camera pictures 0.7 s after release (left) and 1.7 s after release (right). The modeled gate wings (a) were represented by body forces and were accelerated according to the gate wings (A) in the video documentation (Logan and Iverson, 2013). Initially a narrow centered flow front develops due to the opening (b and B on the left) which then widens up laterally. Once the flow front reaches the sidewalls it gets reflected which causes small surface waves that travel transversal to the flow. These surface patterns occurred both in the simulation and in the experiment (b and B on the right).
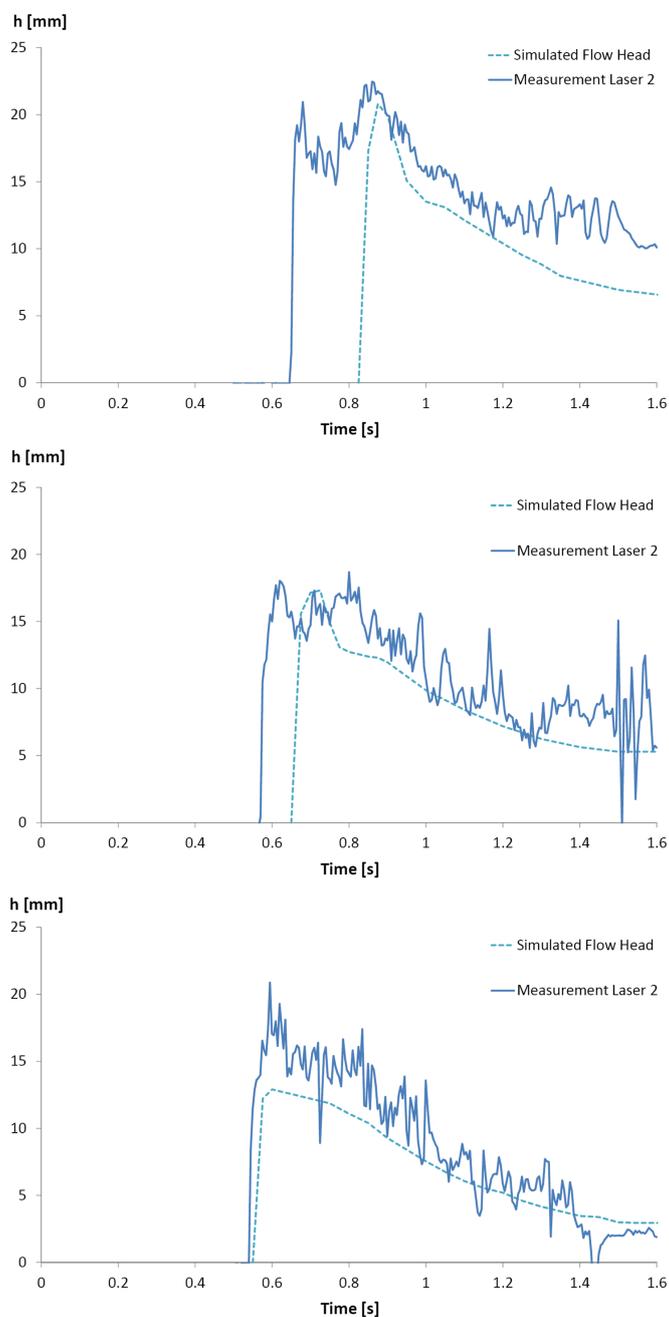
Figure 4. Laser measurement and corresponding simulated values of the flow head over time, one meter down-slope of the gate for experiments with water contents of 27% (top), 28.5% (center) and 30% (bottom). The laser data were box-averaged over 10 milliseconds.
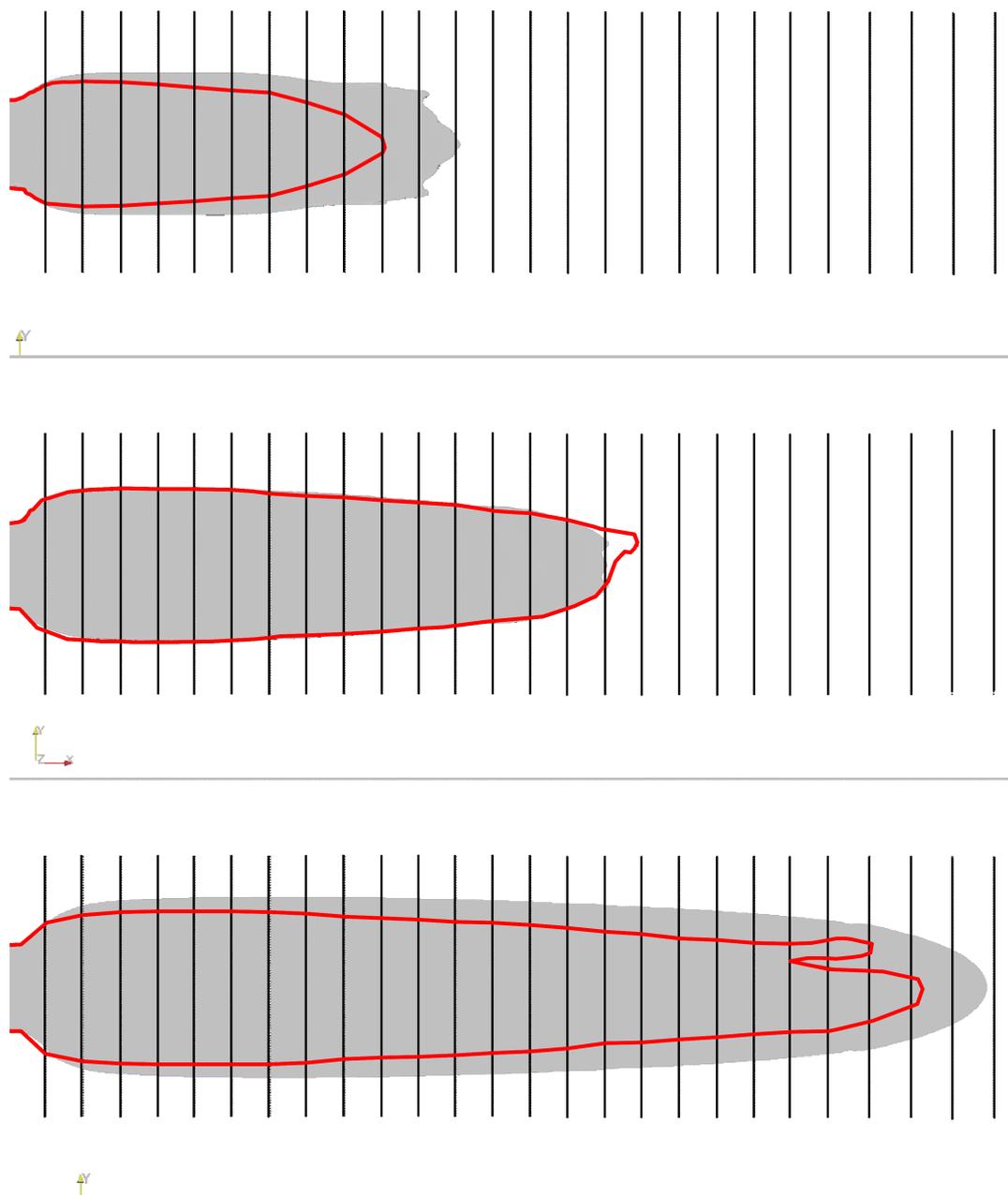
Figure 5. Simulated deposits (gray surface) for the mixture with 27.0% (top), 28.5% (center) and 30% water content (bottom) applying $\delta = 36°$ and τ_{00} based on the calibration case of 28.5% water content. The red outlines indicate the experimental deposits and vertical thin lines represent the 20 cm spacing marks in the experimental slope.
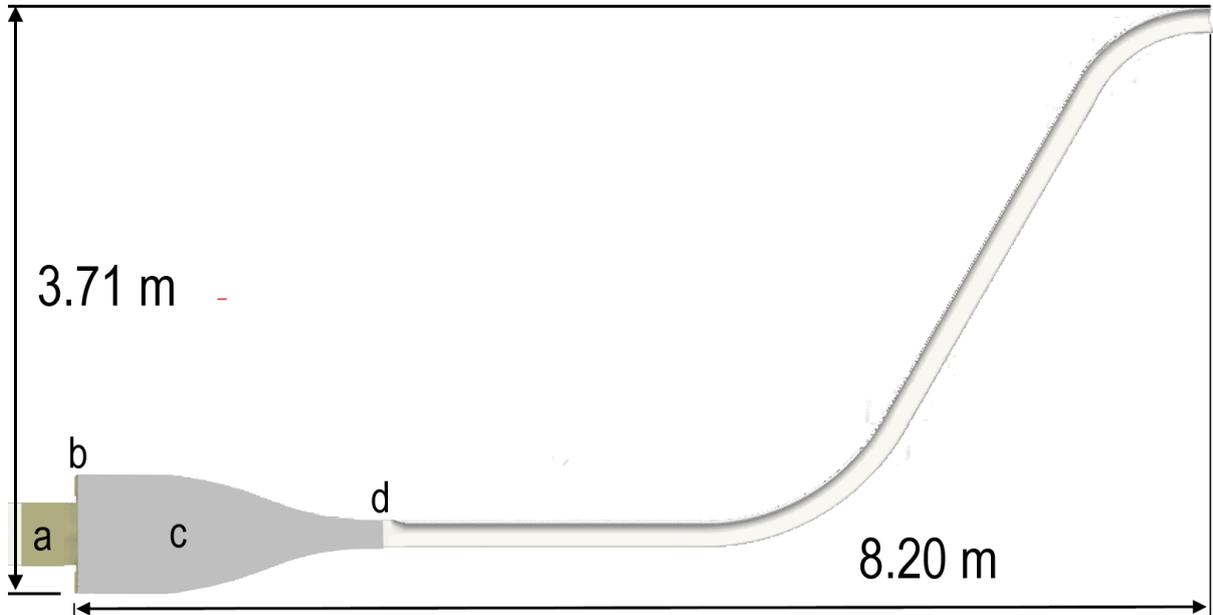
Figure 6. View from top on the modeled curved channel with material released passing from a reservoir (a) through a flap gate (b) into the plane transition box (c). At the restriction (d) the channel profile changes from a rectangle to a half pipe.
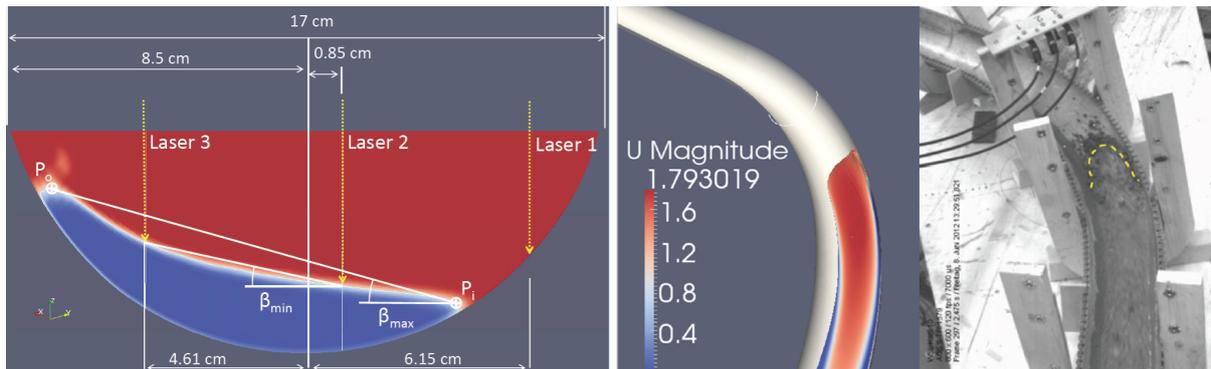
Figure 7. Left: View upstream on modeled channel section 40° after the beginning of the curve, showing air (red), debris mixture (blue), laser positions and minimal and maximal super-elevation angles β. Right: Screen-shot of modeled and experimental flow surface before reaching the laser section at the upper curve. The color bar denotes simulated surface velocity in m/s; the dashed line in the experiment indicates the transition between the granular front and the viscous mixture.
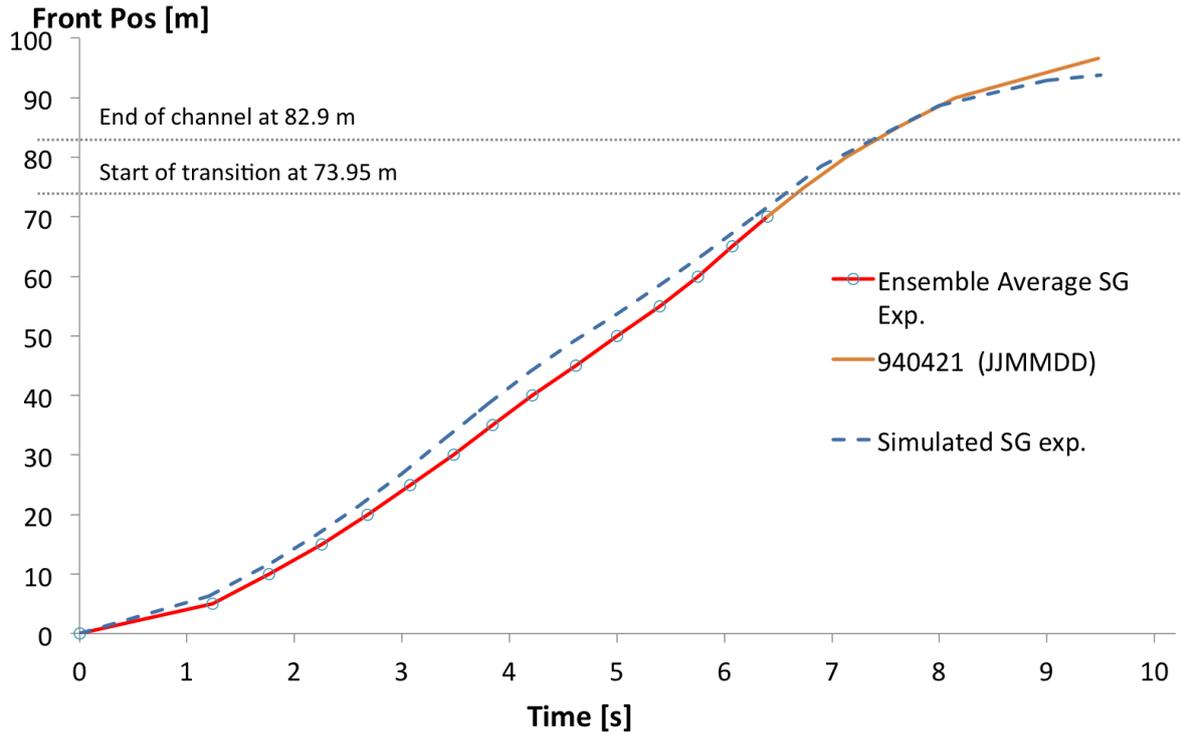
Figure 8. Comparison of the flow front position over time in the smooth-channel SG mixture simulation with the ensemble average front position up to 70 m flow distance as published in Iverson et al. (2010), and a continued comparison for the runout with an experiment from April 1994 (continued graph 940421). The value of $\tau_{00} = 82.8$ Pa derived for the SGM mixture was applied for the SG mixture without recalibration, using the Herschel-Bulkley rheology with 16% water, no clay, 1% silt and 33% sand.
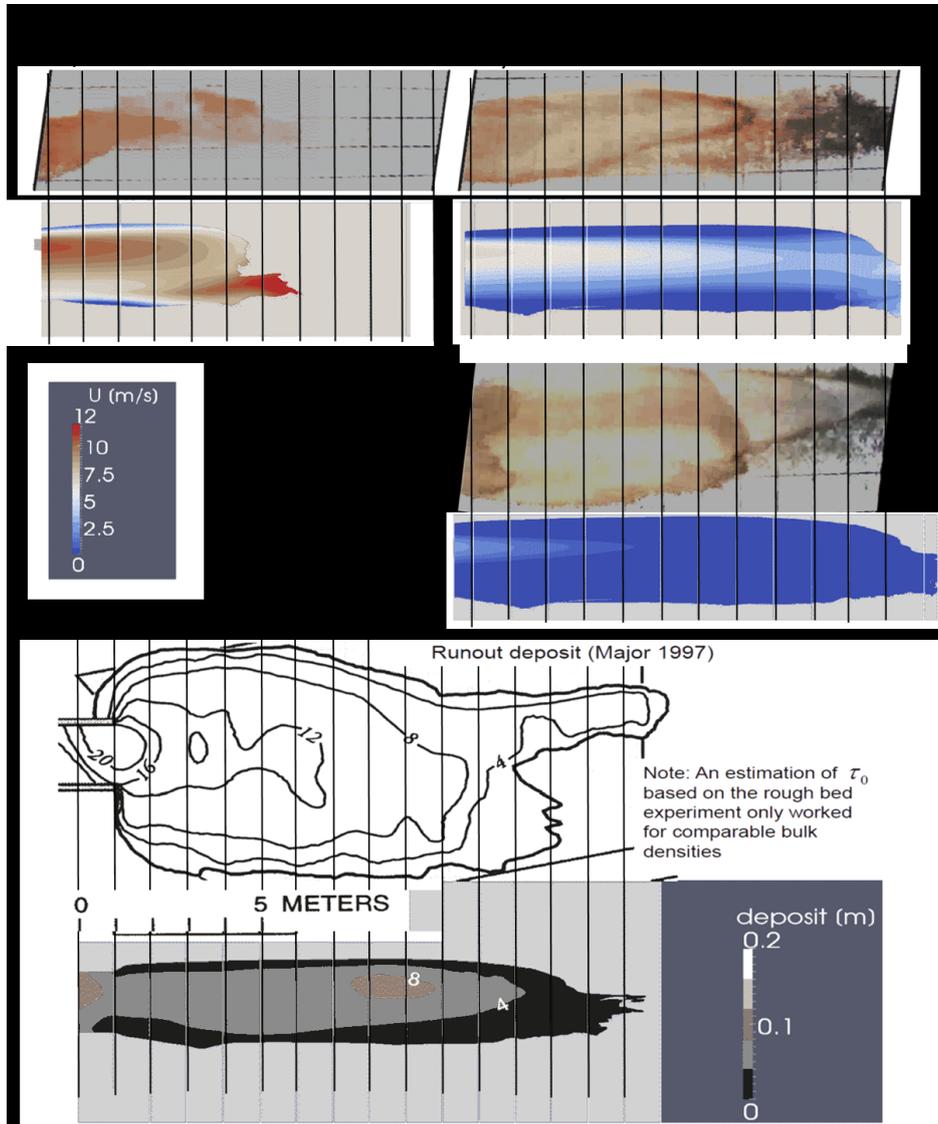
Figure 9. Time-tracking of the run-out process by top camera (top panel) and comparison of the final runout deposit in the experiment and simulation (bottom panel). The corresponding simulated material is colored by flow velocity (top) and deposition thickness (bottom). The free model parameter τ_{00} was calibrated to 90 Pa to fit the arrival time in the simulation to the experiment. The experimental time was derived by counting the number of video frames in the overview camera video between release and arrival in the run-out plane (Logan and Iverson, 2013). The deposit in the experiment widens up as later surges of liquid material meet the first surge deposit and spread to the sides at the beginning of the plane. The simulation only covers a single surge runout with homogeneous (unsorted) material.
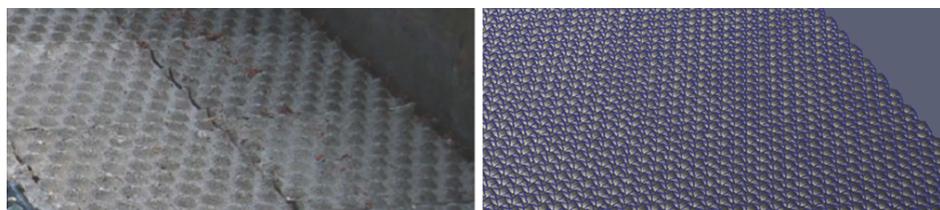
Figure 10. View of the rough channel bed at the experimental site (left) and in the simulation (right). Across the channel width, a larger number of bumps was introduced into the model to combine simple mesh generation with a high grid resolution.
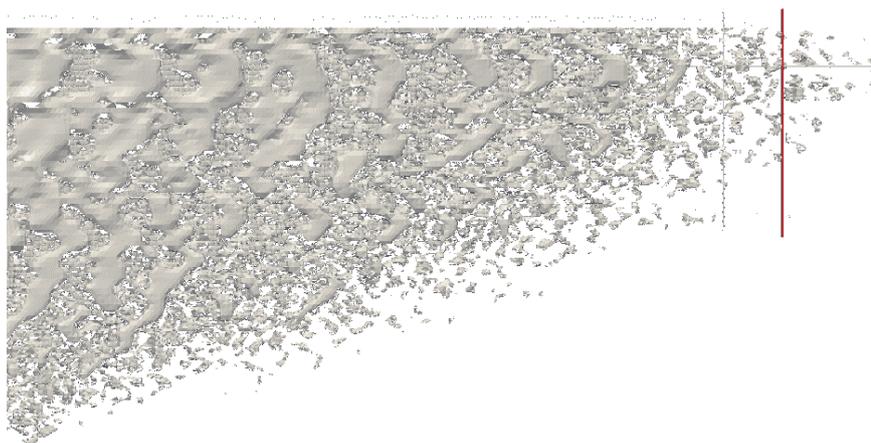
Figure 11. Top view of the modeled flow front, with the transition between air and debris flow material, marked here by the layer with material concentration equal to one third, shown as a free surface. The red bar marks the flow front position presumed as the beginning of the continuous surface. Single drops downstream of this point are not considered as part of the flow front.
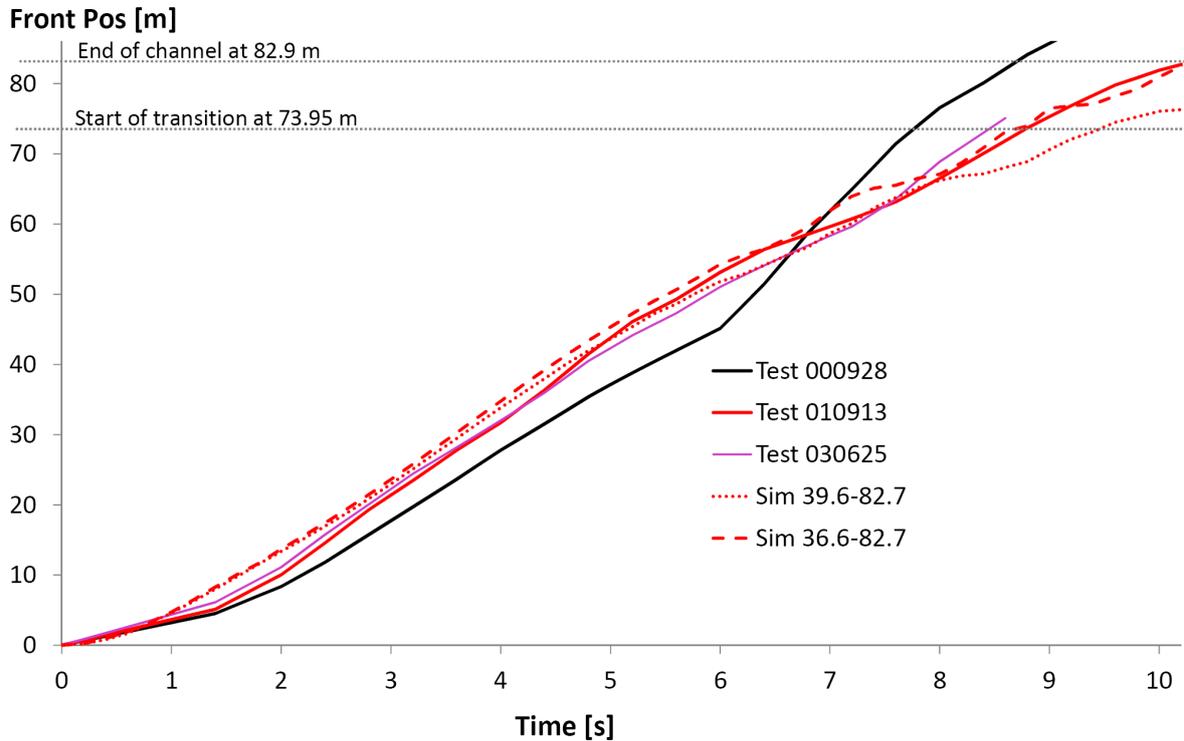
Figure 12. The flow front position over time of the rough-channel SGM mixture simulations, compared to three selected experiments of identical setup using the so-called SGM mixture, a standard mixture of sand, gravel and loam (Iverson et al., 2010). We selected the three tests because the corresponding travel times could be derived from the published figure in Iverson et al. (2010). We investigated the development of the flow front in combination with the video documentation. The three tests experienced increasing front flow velocities after 6 seconds (black graph, test 000928), 7.4 seconds (pink graph, test 030625) and about 7.5 seconds (red, test 010913) as a second surge reached the flow front (observed from video, see Fig. 13). Since the bed roughness is overestimated by a representation as pyramids instead of round-nosed cones, one simulation used a reduced friction angle of $36.6°$ that corresponds to the lower boundary of possible experimental values based on published standard deviations (see Iverson et al. (2010) table 3).

Figure 13. Snapshots of the flow front of test 000928 (left) 5.6 s after release (bottom left) when the approaching second surge (top left) unified with the front. The same happened in test 010913 (center top and center bottom) 7.4 seconds after release and in test 030625 (right top and right bottom) 7.0 seconds after release. The upper row of images capture the moment about half a second earlier in time than the lower row, showing the approaching second surge (indicated by the white arrows and a red line, the surge is more apparent in the video, see Logan and Iverson (2013)). In the lower row, the moments are shown were the second surge reaches the flow front. The corresponding time coincided with a sudden increase in front velocity; see Fig. 12.
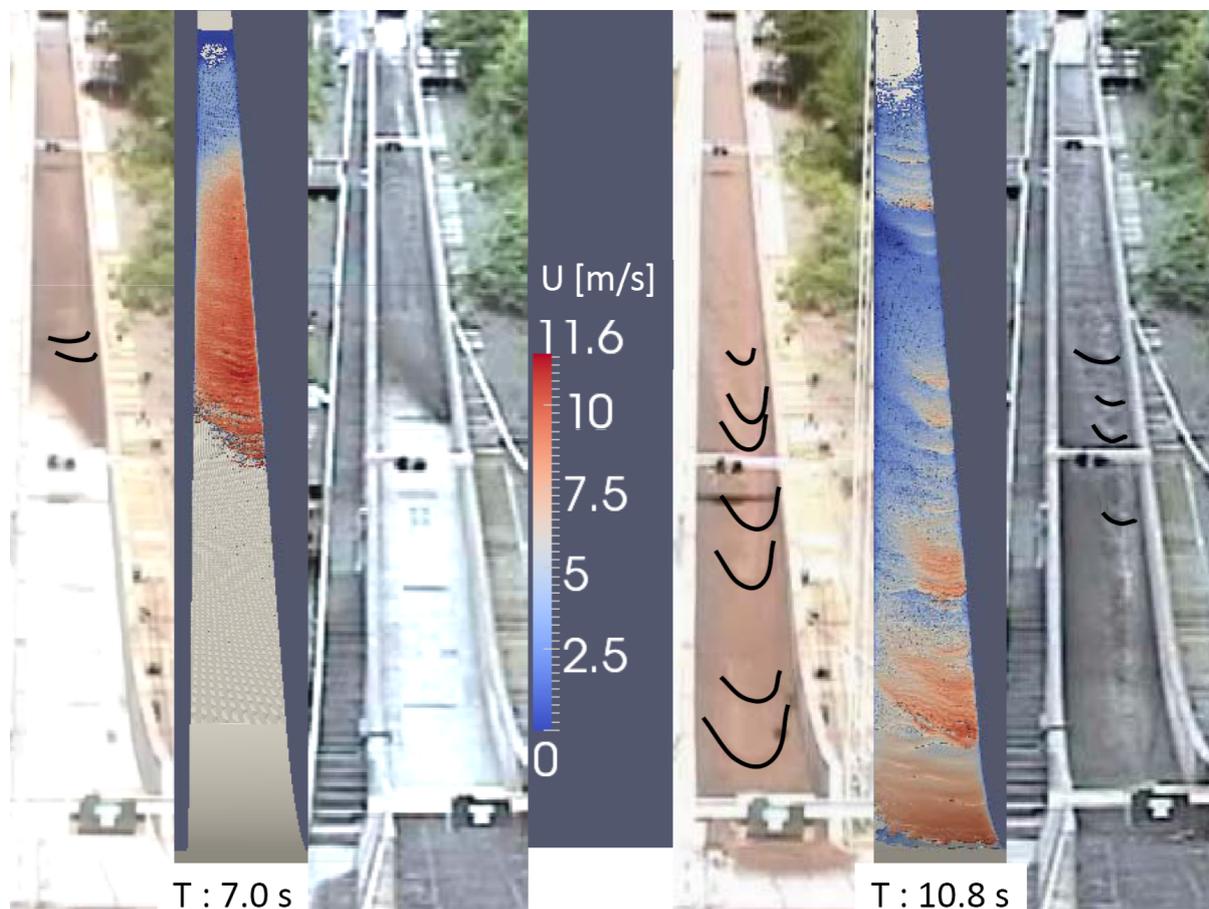
Figure 14. Comparison of the material surface in test 010913 (left of simulation) and test 030625 (right of simulation) at an intermediate position 7 s after release (left) and at the simulated front arrival at the run-out plane at 10.8 s (right) for a modeled friction angle of 36.6°. Black lines in the pictures highlight surface wave fronts, which appear more clearly in the video (Logan and Iverson, 2013). In the simulation such waves are indicated by using the surface velocity as the color scale.
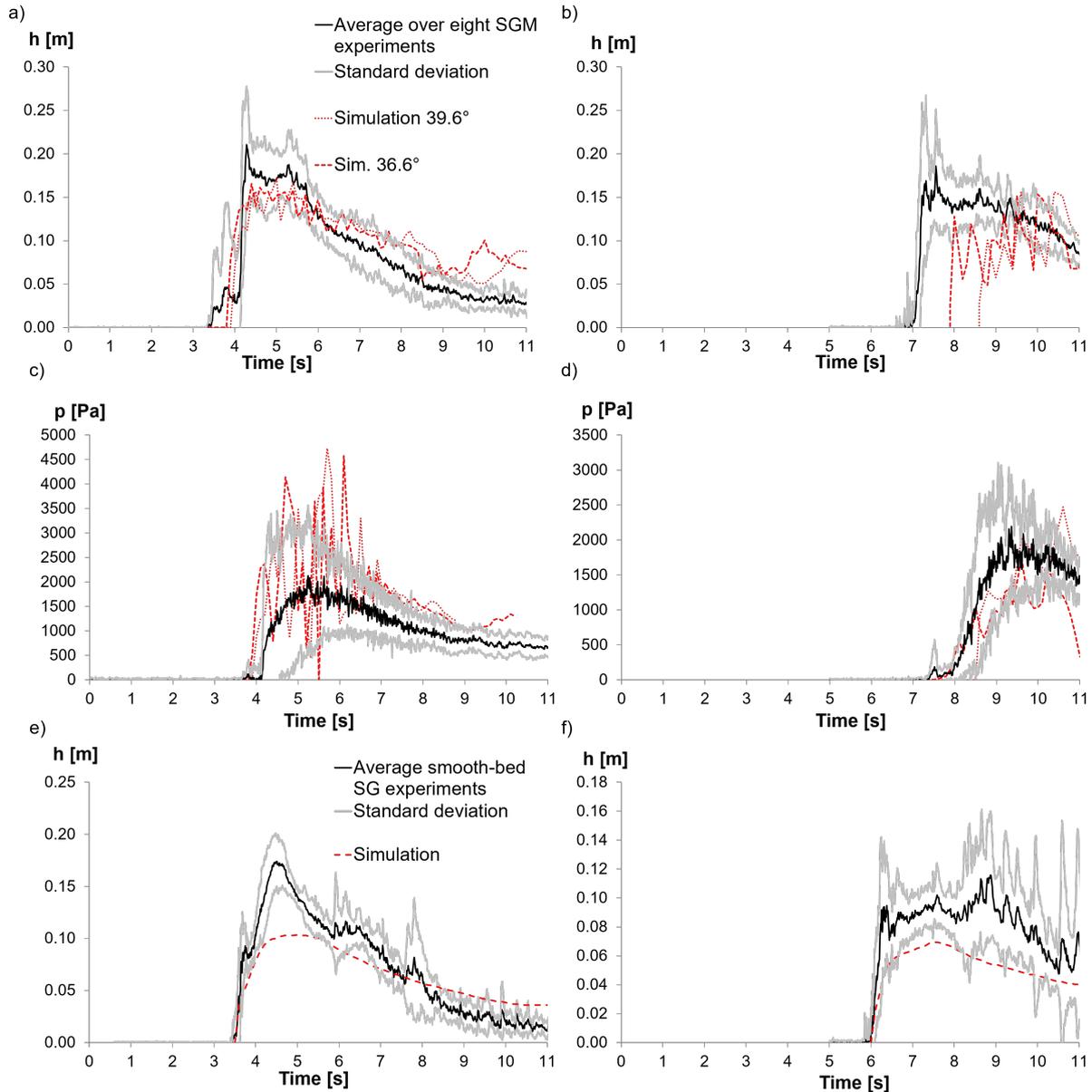
Figure 15. USGS flume experiments compared to the simulation with $\tau_{00} = 82.8$ Pa: (a) and (c) show the flow depth and basal pressures from the ensemble average of eight SGM experiments on the rough channel at a position 32 m downslope of the release gate, and the corresponding simulation results for two gravel friction angles. The diagrams (b) and (d) show the same for a position 66 m downslope, and(e) and (f) show the comparison of simulated and measured flow heights 32 m and 66 m downslope of the release gate for the ensemble average of smooth-channel SG-experiments. The ensemble averages are based on the data published in Iverson et al. (2010). The measured basal normal stresses were derived as the average temporal value of three force plates placed in the channel center line at 31.7, 32.3 and 32.9 m downslope from the release gate (c) and 65.6, 66.2 and 66.8 m downslope (d). The force plates were circular; however, due to the simulation grid geometry, three squares of basal cells with the same areas and positions as the force plates were used to derive the values of basal pressure in the simulation.